Variable-On-Time Control to Achieve High Input Power Factor for a CRM-Integrated Buck–Flyback PFC Converter

Abdul Hakeem Memon, Kai Yao, *Member, IEEE*, Qingwei Chen, Jian Guo, and Wenbin Hu

***Abstract*—A variable-on-time (VOT) control scheme for a critical conduction mode (CRM) integrated buck–flyback power factor correction (PFC) converter with high power factor (PF) and low total harmonic distortion (THD) is proposed in this paper. By utilizing the input and output voltage to modulate the on-time of both buck and flyback switches, the input current harmonics can be eliminated and high PF will be obtained. The operating principles of both the conventional constant-on-time (COT) control and VOT control for the CRM buck–flyback PFC converter are analyzed. A 100-W prototype has been built and tested in the lab. The experimental results demonstrate that the THD and PF of the converter with VOT control are greatly improved compared to those with COT control.**

***Index Terms*—Constant-on-time (COT), critical conduction mode (CRM), power factor correction (PFC), variable-on-time (VOT).**

I. Introduction

FOR achieving high power factor (PF) and low total harmonic distortion (THD), power factor correction (PFC) converters are normally used in most of ac–dc power conversion applications. PFC converters may be divided into active and passive types. Active PFC converters have more advantages as compared to passive ones in terms of high PF and small size [1]. Various types of topologies and control schemes are available to implement the active PFC techniques [2]–[11]. Among them, buck PFC converter is a good choice especially for a broad range of ac/dc applications due to its several advantages like high efficiency, cost reduction, low output voltage, and life time improvement. In literature, many researchers [12]–[24] have introduced the buck PFC converter as a preregulator. The buck ac–dc converter can overcome the disadvantages of the universal input condition. On the other hand, if this converter works in hard switching mode, switching losses will be higher especially at high input voltage that deteriorates the advantages of buck converter [19]. The problem of hard switching mode can be overcome by operating it in critical conduction mode (CRM), which can provide zero voltage switching (ZVS) and reduce reverse recovery losses in diode [19], [20].

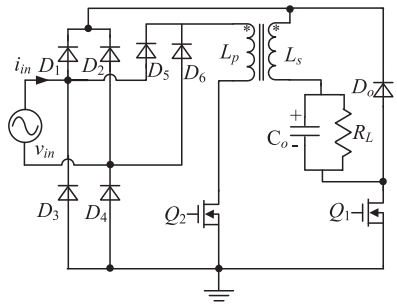

Fig. 1. Main circuit of the buck–flyback PFC converter.

The constant-on-time (COT) control for CRM buck PFC converter was introduced by Yang *et al.* [21] and Wu *et al.* [22]. Because of a dead zone in the input average current which appears while the input voltage is less than output voltage as shown in Fig. 1, it is hard to meet the IEC61000-3-2 criteria. A variable-on-time (VOT) was introduced to increase the PF of the CRM buck PFC converter [23].

A novel integrated buck–flyback PFC converter was proposed to solve the dead zone problem of the buck converter; thus, the PF is improved [24]. Operating with COT control, the average input current shape of this converter is not purely sinusoidal; therefore, the PF is not nearly equal to unity and the THD is still a little high.

In order to achieve nearly unity PF within the wide input voltage range, VOT control for the CRM buck–flyback PFC converter is proposed in this paper. The arrangement of the remaining portion of the paper is as follows. In Section II, the operating principle of the conventional COT control for the CRM buck–flyback PFC converter is studied. In Section III, the VOT control for the converter is put forward so that the PF is improved to unity over the whole input voltage range. Section IV deals with comparison between COT and VOT control in terms of output voltage ripple and power loss analysis. The obtained results on a 100-W prototype of the converter are presented in Section V. Finally, a conclusion is given in Section VI to summarize the paper.

Manuscript received March 3, 2016; revised May 9, 2016 and July 14, 2016; accepted August 29, 2016. Date of publication September 13, 2016; date of current version February 27, 2017. This work was supported in part by the National Natural Science Foundation of China under Grants 51307085, 51677091, and 61673219, and in part by the Excellent Youth Fund project of Jiangsu Natural Science Foundation under Grant BK20160086. Recommended for publication by Associate Editor L. Huber. *(Corresponding author: Kai Yao).*

The authors are with the School of Automation, Nanjing University of Science and Technology, Nanjing 210094, China (e-mail: engrahm87@yahoo.com; yaokai@njust.edu.cn; cqw1002@sina.com; guoj1002@njust.edu.cn; hwb_njust@163.com).

Color versions of one or more of the figures in this paper are available online at http://ieeexplore.ieee.org.

Digital Object Identifier 10.1109/TPEL.2016.2608839

II. Conventional COT Control for the CRM Buck–Flyback PFC Converter

Fig. 1 shows the main circuit of the buck–flyback PFC converter. The converter operates in the buck mode when the input voltage is more than the boundary voltage and vice versa in the flyback mode. The boundary voltage is set a little higher than the output voltage. Thus, there are two cases for the converter.

The input voltage is given by

$$v_{\rm in}(\theta) = V_m \sin\theta \tag{1}$$

where V_m is the amplitude and θ is the angle of the input voltage.

When $v_{\rm in} > V_{\rm boundary}$, the converter operates in the buck mode, the switch Q_1 keeps switching and the switch Q_2 is OFF.

While Q_1 is ON, the voltage across the secondary inductor is given by

$$L_s \frac{di_s}{dt} = V_m \left|\sin\theta\right| - V_o \;\; (\theta_0 \le \theta \le \pi - \theta_0). \tag{2}$$

Therefore, the peak value of secondary inductor current is

$$i_{\rm Ls\_pk}(\theta) = \frac{V_m \left|\sin\theta\right| - V_o}{L_s} t_{\rm on} \tag{3}$$

where $t_{\rm on}$ is the on-time of the switch.

When Q_1 is OFF, the secondary inductor is discharged by V_o

$$-L_s \frac{di_s}{dt} = V_o. \tag{4}$$

Hence, the peak value of secondary inductor current is

$$i_{\rm Ls\_pk}(\theta) = \frac{V_o}{L_s} t_{\rm off}. \tag{5}$$

According to the volt–second balance, the relationship between $t_{\rm off}$ and $t_{\rm on}$ is

$$t_{\rm off} = \frac{V_m \left|\sin\theta\right| - V_o}{V_o} t_{\rm on}. \tag{6}$$

Also

$$t_s = t_{\rm on} + t_{\rm off}. \tag{7}$$

Combining (6) and (7)

$$t_s = \frac{V_m \left|\sin\theta\right|}{V_o} t_{\rm on}. \tag{8}$$

The average input current of the buck converter is derived as

$$i_{b\_\rm avg}(\theta) = \frac{i_{\rm Ls\_pk}(\theta) t_{\rm on}}{2t_s}. \tag{9}$$

Substitution of (3) and (8) into (9) leads to

$$i_{b\_\rm avg}(\theta) = \frac{t_{\rm on} V_o}{2L_s} \left(\frac{V_m \left|\sin\theta\right| - V_o}{V_m \left|\sin\theta\right|}\right) (\theta_0 \le \theta \le \pi - \theta_0). \tag{10}$$

When $v_{\rm in} < V_{\rm boundary}$, the converter operates in the flyback mode, Q_2 keeps switching and Q_1 is OFF.

While Q_2 is ON, the voltage across the primary inductor is

$$L_p \frac{di_{\rm Lp}}{dt} = V_m \left|\sin\theta\right| \quad (0 \le \theta < \theta_0 \,\&\, \pi - \theta_0 < \theta \le \pi). \tag{11}$$

Thus, the peak value of primary inductor current is given by

$$i_{\rm Lp\_pk}(\theta) = \frac{V_m \left|\sin(\theta)\right|}{L_p} t_{\rm on}. \tag{12}$$

When Q_2 is OFF, the secondary inductor is discharged by V_o

$$-L_s \frac{di_s}{dt} = V_o \tag{13}$$

$$i_{\rm Ls\_pk}(\theta) = \frac{V_o}{L_s} t_{\rm off}. \tag{14}$$

According to the volt–second balance, the following equation can be obtained:

$$t_{\rm off} = \frac{\sqrt{L_s} V_m \left|\sin\theta\right|}{\sqrt{L_p} V_o} t_{\rm on}. \tag{15}$$

Combining (7) and (15) leads to

$$t_s = \left(1 + \frac{\sqrt{L_s} V_m \left|\sin\theta\right|}{\sqrt{L_p} V_o}\right) t_{\rm on}. \tag{16}$$

The average input current of the flyback converter can be expressed as

$$i_{f\_\rm avg}(\theta) = \frac{i_{\rm Lp\_pk}(\theta) t_{\rm on}}{2t_s}. \tag{17}$$

Substitution of (12) and (16) into (17) results in

$$i_{f\_\rm avg}(\theta) = \frac{t_{\rm on} V_m \left|\sin\theta\right|}{2L_p \left(1 + \frac{\sqrt{L_s} V_m \left|\sin\theta\right|}{\sqrt{L_p} V_o}\right)} \quad (0 \le \theta < \theta_0 \,\&\, \pi - \theta_0 < \theta \le \pi). \tag{18}$$

According to the above analysis, the average input current of the converter with COT control is

$$i_{\rm in\_COT}(\theta) = \begin{cases} \dfrac{t_{\rm on} V_m \left|\sin\theta\right|}{2L_p \left(1 + \dfrac{\sqrt{L_s} V_m \left|\sin\theta\right|}{\sqrt{L_p} V_o}\right)} \\ \qquad (0 \le \theta < \theta_0 \,\&\, \pi - \theta_0 < \theta \le \pi) \\ \dfrac{t_{\rm on} V_o}{2L_s} \left(\dfrac{V_m \left|\sin\theta\right| - V_o}{V_m \left|\sin\theta\right|}\right) (\theta_0 \le \theta \le \pi - \theta_0) \end{cases}. \tag{19}$$

Combining (1) and (19), the average input power can be calculated as

$$\begin{aligned} P_{\rm in} &= \frac{1}{\pi} \int_0^{\pi} v_{\rm in}(\theta) i_{\rm in}(\theta) d\theta \\ &= \frac{1}{\pi} \left[\int_0^{\theta_0} \frac{t_{\rm on} (V_m \left|\sin\theta\right|)^2}{L_p \left(1 + \dfrac{\sqrt{L_s} V_m \left|\sin\theta\right|}{\sqrt{L_p} V_o}\right)} d\theta + \int_{\theta_0}^{\pi/2} \frac{V_o t_{\rm on} \left(V_m \left|\sin\theta\right| - V_o\right)}{L_s} d\theta \right]. \end{aligned} \tag{20}$$

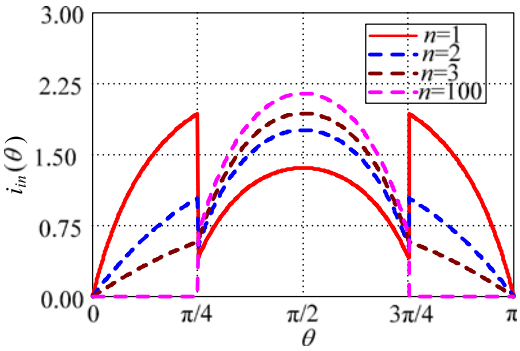

Fig. 2. Average input current waveform for different n at 90 VAC.

If the efficiency of the converter is assumed to be 100%, i.e. $P_{\text{in}} = P_o$, then t_{on} for COT control is derived as

$$t_{\text{on}} = \frac{\pi P_o}{\left[\int_0^{\theta_0} \frac{(V_m |\sin\theta|)^2}{L_p\left(1+\frac{\sqrt{L_s}V_m|\sin\theta|}{\sqrt{L_p}V_o}\right)}d\theta + \int_{\theta_0}^{\pi/2} \frac{V_o(V_m|\sin\theta|-V_o)}{L_s}d\theta\right]}. \tag{21}$$

Combining (19), (21), and the specifications of the converter, we can plot the average input current waveform at 90 VAC for different turns ratio between the primary and secondary sides, i.e., $n = 1$, 2, 3, and 100, as shown in Fig. 2.

It is clear that the shape of average input current is not purely sinusoidal. Hence, whatever the turns ratio is, for COT control, the unity PF cannot be achieved.

III. Proposed VOT Control to Improve the Input PF

A. VOT Control for Unity PF

By considering (10), for achieving a unity PF, the on-time of buck switch Q_1 can be variable as

$$t_{\text{on\_buck}} = k_{\text{on1}} \frac{(V_m|\sin\theta|)^2}{V_o(V_m|\sin\theta| - V_o)} \tag{22}$$

where k_{on1} is a constant.

According to (10) and (22), the average input current of buck converter is

$$i_{b\_\text{avg}}(\theta) = \frac{k_{\text{on1}}V_m|\sin\theta|}{2L_p}(\theta_0 \le \theta \le \pi - \theta_0). \tag{23}$$

By observing (18), for obtaining a unity PF, the on-time of flyback switch Q_2 varies as

$$t_{\text{on\_flyback}} = k_{\text{on2}}\left(1+\frac{\sqrt{L_s}V_m|\sin\theta|}{\sqrt{L_p}V_o}\right) \tag{24}$$

whereas k_{on2} is a constant.

By substituting (24) into (18), the average input current of flyback converter is

$$i_{f\_\text{avg}}(\theta) = \frac{k_{\text{on2}}V_m|\sin\theta|}{2L_p}(0 \le \theta < \theta_0 \,\&\, \pi - \theta_0 < \theta \le \pi). \tag{25}$$

The average input current of the converter with VOT control is

$$i_{\text{in\_VOT}}(\theta) = \begin{cases} \frac{k_{\text{on2}}V_m|\sin\theta|}{2L_p} & (0 \le \theta < \theta_0 \,\&\, \pi - \theta_0 < \theta \le \pi) \\ \frac{k_{\text{on1}}V_m|\sin\theta|}{2L_s} & (\theta_0 \le \theta \le \pi - \theta_0) \end{cases} \tag{26}$$

Due to the power balance between the input and output, for unity PF, the input current can be written as

$$i_{\text{in}}(\theta) = \frac{2P_o|\sin\theta|}{V_m}. \tag{27}$$

From (26) and (27), the input current at θ_0 is

$$i_{\text{in}}(\theta_0) = \frac{k_{\text{on1}}V_m|\sin\theta_0|}{2L_s} = \frac{k_{\text{on2}}V_m|\sin\theta_0|}{2L_p} = \frac{2P_o|\sin\theta_0|}{V_m}. \tag{28}$$

Therefore

$$k_{\text{on1}} = \frac{4P_oL_s}{V_m^2} \tag{29}$$

$$k_{\text{on2}} = \frac{4P_oL_p}{V_m^2}. \tag{30}$$

Substitution of (29) and (30) into (22) and (24) leads to

$$t_{\text{on}}(\theta) = \begin{cases} \frac{4P_oL_p}{V_m^2}\left(1+\frac{\sqrt{L_s}V_m|\sin\theta|}{\sqrt{L_p}V_o}\right) \\ \qquad (0 \le \theta < \theta_0 \,\&\, \pi - \theta_0 < \theta \le \pi) \\ \frac{4P_oL_s\sin^2\theta}{V_o(V_m|\sin\theta| - V_o)} \quad (\theta_0 \le \theta \le \pi - \theta_0) \end{cases}. \tag{31}$$

Equations (26), (29), and (30) clearly show that unity input PF will be achieved by using proposed VOT control for the buck–flyback PFC converter at all turns ratios.

B. Implementation of Control Scheme

Fig. 3 illustrates the complete control block diagram for the CRM buck–flyback PFC converter.

The VOT control scheme for the buck PFC converter is shown in the area of the red dotted line. The rectified input voltage $v_{g1} = V_m|\sin\theta|$ is sensed through a voltage divider circuit of R_5 and R_6

$$k_1 = \frac{R_6}{R_5 + R_6} \tag{32}$$

where k_1 is the voltage sensor gain R_1, R_2, R_3, R_4 and *FMMT* 560 senses the output voltage, and the gain is

$$k_3 = \frac{R_4\left(\frac{R_1V_o}{R_1+R_2} - V_{\text{eb}}\right)}{R_3V_o} \tag{33}$$

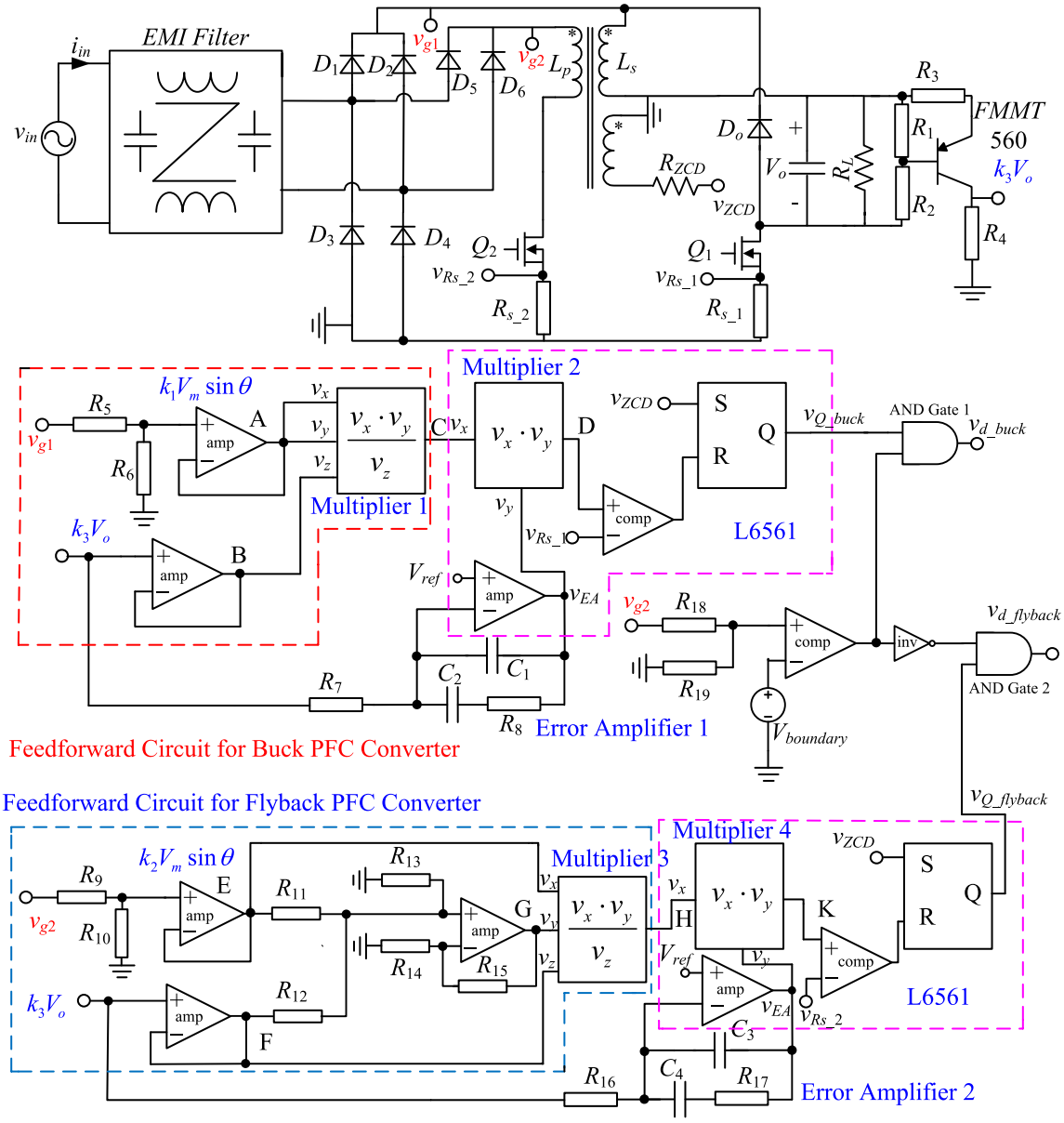

Fig. 3. Control diagram.

where $V_{\rm eb}$ is the voltage drop between emitter and base of the transistor.

According to Fig. 3, the inputs to multiplier 1 are given by

$$v_x = k_1 v_{g1} \tag{34}$$

$$v_y = k_1 v_{g1} \tag{35}$$

$$v_z = k_3 V_o. \tag{36}$$

The output of multiplier 1 is

$$v_C = \frac{k_1^2 v_{g1}^2}{k_3 V_o}. \tag{37}$$

The error amplifier 1 regulates the output voltage. The sensed output voltage is compared with the reference voltage $V_{\rm ref}$ which is set as 2.5 V and the sense gain k_3 is set at 0.0132. R_7, C_2, R_8, C_1 form the compensation network. $v_{\rm EA}$ and $v_{\rm C}$ are sent to multiplier 2, whose output is

$$v_D = v_{\rm EA\_buck} \frac{k_1^2 v_{g1}^2}{k_3 V_o}. \tag{38}$$

The current of buck switch is sensed through a series resistor R_{s_1}. v_D and the sensed current of buck switch are sent to the comparator. The output of comparator and ZCD drives the buck switch to work with VOT control. The on-time of the switches Q_1 is decided by v_D in the control block.

When Q_1 is ON, the voltage across the current sensor resistor of secondary inductor in the main circuit is

$$v_{\rm Rs\_1} = \frac{V_m \left|\sin\theta\right| - V_o}{L_s} t_{\rm on}. \tag{39}$$

The current through secondary inductor increases until the time instant when $v_{\mathrm{RS\_1}}$ equals v_D expressed in (38); therefore

$$t_{\mathrm{on\_buck}} = \frac{k_1^2 v_{\mathrm{EA\_buck}} L_s}{k_3} \frac{(V_m |\sin\theta|)^2}{V_o (V_m |\sin\theta| - V_o)}. \quad (40)$$

It is obvious that the variation rule of t_{on} in (40) is the same with the theoretical expression of (22) which was proposed in Section III-A. Also, it can be derived from (40) and (22) that

$$v_{\mathrm{EA\_buck}} = \frac{k_{\mathrm{on1}} k_3}{k_1^2 L_s}. \quad (41)$$

Therefore, v_{EA} can be obtained by substituting (29) in (41)

$$v_{\mathrm{EA\_buck}} = \frac{k_{\mathrm{on1}} k_3}{k_1^2 L_s}. \quad (42)$$

The error amplifier will adjust itself to achieve the required output voltage. Although P_o, V_m and k_1 and k_3 are certain, (42) is the actual value of the error amplifier output.

The VOT control scheme for the flyback PFC converter is shown in the area of the blue dotted line in Fig. 3. The voltage sensor circuit composed of R_9 and R_{10} senses the rectified input voltage $v_{g2} = V_m |\sin\theta|$, whose gain is

$$k_2 = \frac{R_{10}}{R_9 + R_{10}}. \quad (43)$$

From Fig. 3, v_x input of multiplier 3 is

$$v_x = k_2 v_{g2}. \quad (44)$$

If $R_{11} = R_{12} = R_{13} = R_{15} = 2R_{14}$, then

$$v_y = k_2 v_{g2} + k_3 V_o. \quad (45)$$

Also

$$v_z = k_3 V_o. \quad (46)$$

The output of multiplier 3 can be expressed as

$$v_H = \frac{k_2 v_{g2} (k_2 v_{g2} + k_3 V_o)}{k_3 V_o}. \quad (47)$$

The same as error amplifier 1, v_{EA} and v_H are given to multiplier 4, whose output can be expressed as

$$v_K = v_{\mathrm{EA}} \frac{k_2 v_{g2} (k_2 v_{g2} + k_3 V_o)}{k_3 V_o}. \quad (48)$$

The current of flyback switch is sensed through a series resistor R_{s_2}. v_K and the sensed current of flyback switch are given to the comparator. The output of comparator and ZCD drives the flyback switch to work with VOT control. The on-time of the switches Q_2 is decided by v_K in the control block.

When Q_2 is ON, the voltage across the current sensor resistor of primary inductor in the main circuit is

$$v_{\mathrm{Rs\_2}} = \frac{V_m |\sin\theta|}{L_p} t_{\mathrm{on}} \quad (49)$$

$v_{\mathrm{RS\_2}}$ increases with the current and when it reaches the value of v_K expressed in (48), Q_2 will turn OFF. The on-time of Q_2 is obtained by combining (48) and (49)

$$t_{\mathrm{on\_flyback}} = k_2 v_{\mathrm{EA\_flyback}} L_p \left(1 + \frac{k_2 V_m |\sin\theta|}{k_3 V_o}\right) \quad (50)$$

R_9 and R_{10} are selected to let $k_2 = k_3 \sqrt{\frac{L_s}{L_p}}$, then it is clear that (50) is the same in form as (24) which was proposed in Section III-A. Also, it can be derived from (50) and (24) that

$$v_{\mathrm{EA\_flyback}} = \frac{k_{\mathrm{on2}}}{k_2 L_p}. \quad (51)$$

Further, v_{EA} can be obtained by substituting (30) in (51)

$$v_{\mathrm{EA\_flyback}} = \frac{4P_o}{k_2 V_m^2}. \quad (52)$$

The error amplifier will adjust itself to achieve the required output voltage. Although P_o, V_m, and k_2 are certain, (52) is the actual value of the error amplifier output.

From the abovementioned analysis, we can see that the control block can realize the unity PF with any turns ratio for the converter.

IV. Comparative Analysis of COT and VOT Control for the CRM Buck–Flyback PFC Converter

A. Output Voltage Ripple

Output voltage ripple of the converter with COT and VOT controls can be expressed as

$$\Delta V_{o\_\mathrm{COT}} = \frac{2P_o \int_0^{\theta_1} \left[1 - \frac{v_{\mathrm{in}}(\theta)\, i_{\mathrm{in\_COT}}(\theta)}{P_o}\right] d\theta}{\omega C_o V_o} \quad (53)$$

$$\Delta V_{o\_\mathrm{VOT}} = \frac{2P_o \int_0^{\pi/4} \left[1 - \frac{v_{\mathrm{in}}(\theta) i_{\mathrm{in\_VOT}}(\theta)}{P_o}\right] d\theta}{\omega C_o V_o} \in . \quad (54)$$

Based on (1), (19), (21), (26), (29), (30), (53), and (54), and specifications of the converter, $\Delta V_{o\_\mathrm{COT}}$ and $\Delta V_{o\_\mathrm{VOT}}$ can be figured out as illustrated in Fig. 4. It demonstrates that for $n = 1$, the output voltage ripple of the converter with VOT control is slightly larger than that with COT control, whereas for $n = 2$, the ripple with VOT control is slightly lower than that with COT control at low input voltage and vice versa at high input voltage.

B. Power Losses Analysis

The rms current of the ON time period, i.e., the rms current of switch Q_1 and Q_2 can be calculated respectively as

$$I_{\mathrm{rms\_}Q_1\mathrm{\_on}} = \sqrt{\frac{\int_{\theta_0}^{\pi-\theta_0} i_{s\_\mathrm{pk}}^2(\theta) \frac{t_{\mathrm{on}}}{t_s} d\theta}{3\pi}} \quad (55)$$

$$I_{\mathrm{rms\_}Q_2\mathrm{\_on}} = \sqrt{\frac{2\int_0^{\theta_0} i_{p\_\mathrm{pk}}^2(\theta) \frac{t_{\mathrm{on}}}{t_s} d\theta}{3\pi}}. \quad (56)$$

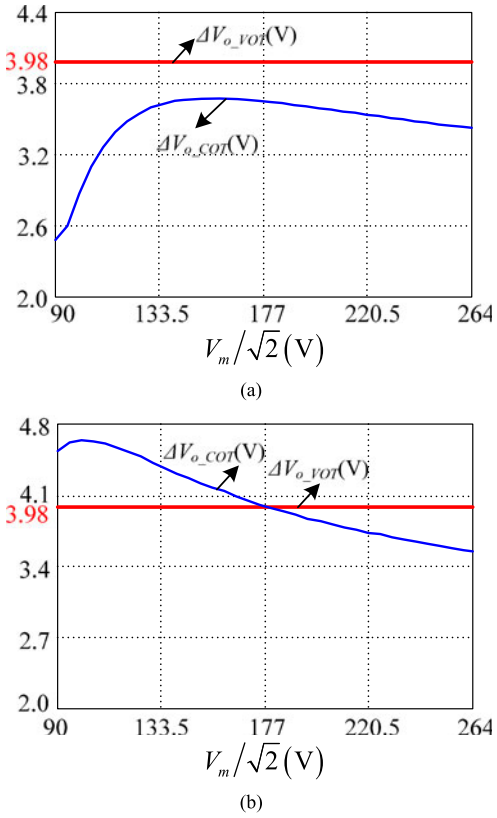

Fig. 4. Calculated output voltage ripple: (a) $n = 1$ and (b) $n = 2$.

The rms current of the off time period is calculated respectively as

$$I_{\text{rms\_}Q_1\text{\_off}} = \sqrt{\frac{\int_{\theta_0}^{\pi-\theta_0} i_{s\_\text{pk}}^2(\theta)\left(1-\frac{t_{\text{on}}}{t_s}\right)d\theta}{3\pi}} \tag{57}$$

$$I_{\text{rms\_}Q_2\text{\_off}} = \sqrt{\frac{2\int_{0}^{\theta_0} i_{p\_\text{pk}}^2(\theta)\left(1-\frac{t_{\text{on}}}{t_s}\right)d\theta}{3\pi}}. \tag{58}$$

While Q_2 is ON, the current flows through the primary winding of the inductor, whose rms current is

$$I_{p\_\text{rms\_COT}} = I_{\text{rms\_}Q_2\text{\_on\_COT}} \tag{59}$$

$$I_{p\_\text{rms\_VOT}} = I_{\text{rms\_}Q_2\text{\_on\_VOT}}. \tag{60}$$

While Q_2 is OFF, and Q_1 is ON and OFF, the current flows through the secondary winding of the inductor, whose rms current is

$$I_{s\_\text{rms\_COT}} = \sqrt{I_{\text{rms\_}Q_1\text{\_on\_COT}}^2 + I_{\text{rms\_}Q_1\text{\_off\_COT}}^2 + I_{\text{rms\_}Q_2\text{\_off\_COT}}^2} \tag{61}$$

$$I_{s\_\text{rms\_VOT}} = \sqrt{I_{\text{rms\_}Q_1\text{\_on\_VOT}}^2 + I_{\text{rms\_}Q_1\text{\_off\_VOT}}^2 + I_{\text{rms\_}Q_2\text{\_off\_VOT}}^2}. \tag{62}$$

1) *Rectifier bridge loss:* Rectifier bridge loss of the converter with COT and VOT controls can be obtained as

$$P_{\text{con\_bridge(COT)}} = \frac{2V_{\text{FD}}}{\pi}\int_0^{\pi} i_{\text{in\_COT}}(\theta)\,d\theta \tag{63}$$

$$P_{\text{con\_bridge(VOT)}} = \frac{2V_{\text{FD}}}{\pi}\int_0^{\pi} i_{\text{in\_VOT}}(\theta)\,d\theta. \tag{64}$$

The value of V_{FD} can be found from the datasheet of KBL10 bridge rectifier. By substituting (19), (21), (26), and (29) and (30) into (63) and (64), rectifier bridge loss can be obtained.

2) *Conduction losses of switch Q_1 and Q_2*: The conduction losses of switch Q_1 and Q_2 with COT and VOT controls can be calculated as

$$\begin{aligned} P_{\text{con\_switches(COT)}} &= I_{\text{rms\_}Q_1\text{\_on\_COT}}^2 R_{\text{DS(on)\_}Q_1} \\ &\quad + I_{\text{rms\_}Q_2\text{\_on\_COT}}^2 R_{\text{DS(on)\_}Q_2} \end{aligned} \tag{65}$$

$$\begin{aligned} P_{\text{con\_switches(VOT)}} &= I_{\text{rms\_}Q_1\text{\_on\_VOT}}^2 R_{\text{DS(on)\_}Q_1} \\ &\quad + I_{\text{rms\_}Q_2\text{\_on\_VOT}}^2 R_{\text{DS(on)\_}Q_2} \end{aligned} \tag{66}$$

where $R_{\text{DS(ON)\_}Q1}$ and $R_{\text{DS(ON)\_}Q2}$ are the on-state resistances of Q_1 and Q_2 whose value can be found from the datasheet of MOSFET 20N60C3. Substituting (3), (8), (12), (16), (21), (31), (55), and (56) into (65) and (66), the conduction losses are achieved.

3) *Turn OFF loss of Q_1 and Q_2*: Due to CRM, the transistors Q_1 and Q_2 turn ON with zero current, and the turn-on loss is nearly negligible. Therefore, the switching loss is mainly the turn-off loss, which can be calculated as follows for COT and VOT control respectively, according to (25) in the application note of Infineon [25, p. 25]

$$\begin{aligned} &P_{\text{off\_switches\_COT}} \\ &= \frac{1}{\pi}\left[\begin{array}{l} 2\int_0^{\theta_0}\begin{pmatrix} E_{\text{off}}(i_{\text{Lp\_pk\_COT}}(\theta))\cdot \\ CF_{\text{off}}(V_{\text{ds}}(off_{\text{flyback}}))\cdot \\ CF_{\text{off}}(R_{\text{gate}})\cdot f_{s\_\text{flyback\_COT}}(\theta)\end{pmatrix}d\theta \\ +\int_{\theta_0}^{\pi-\theta_0}\begin{pmatrix} E_{\text{off}}(i_{\text{Ls\_pk\_COT}}(\theta))\cdot \\ CF_{\text{off}}(V_{\text{ds}}(off_{\text{buck}}))\cdot \\ CF_{\text{off}}(R_{\text{gate}})\cdot f_{s\_\text{buck\_COT}}(\theta)\end{pmatrix}d\theta \end{array}\right] \end{aligned} \tag{67}$$

$$\begin{aligned} &P_{\text{off\_switches\_VOT}} \\ &= \frac{1}{\pi}\left[\begin{array}{l} 2\int_0^{\theta_0}\begin{pmatrix} E_{\text{off}}(i_{\text{Lp\_pk\_VOT}}(\theta))\cdot \\ CF_{\text{off}}(V_{\text{ds}}(off_{\text{flyback}}))\cdot \\ CF_{\text{off}}(R_{\text{gate}})\cdot f_{s\_\text{flyback\_VOT}}(\theta)\end{pmatrix}d\theta \\ +\int_{\theta_0}^{\pi-\theta_0}\begin{pmatrix} E_{\text{off}}(i_{\text{Ls\_pk\_VOT}}(\theta))\cdot \\ CF_{\text{off}}(V_{\text{ds}}(off_{\text{buck}}))\cdot \\ CF_{\text{off}}(R_{\text{gate}})\cdot f_{s\_\text{buck\_VOT}}(\theta)\end{pmatrix}d\theta \end{array}\right] \end{aligned} \tag{68}$$

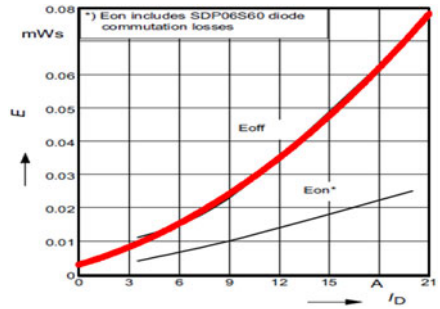

Fig. 5. Curve of the relationship between $E_{\rm off}$ and the current.

whereas switching frequency $f_s(\theta)$ from (8), (16), (21), and (31) for COT and VOT control can be expressed as

$$f_{s\_\rm COT}(\theta)=\begin{cases}\dfrac{V_o\left(\begin{array}{l}\int_0^{\theta_0}\frac{V_o(V_m|\sin\theta|)^2}{V_o+V_m|\sin\theta|}d\theta\\+\int_{\theta_0}^{\pi/2}V_o\left(V_m|\sin\theta|-V_o\right)d\theta\end{array}\right)}{\pi P_o L(V_o+V_m|\sin\theta|)}\\(0\le\theta<\theta_0\,\&\,\pi-\theta_0<\theta\le\pi)\\\dfrac{V_o\left(\begin{array}{l}\int_0^{\theta_0}\frac{V_o(V_m|\sin\theta|)^2}{V_o+V_m|\sin\theta|}d\theta\\+\int_{\theta_0}^{\pi/2}V_o\left(V_m|\sin\theta|-V_o\right)d\theta\end{array}\right)}{\pi P_o LV_m|\sin\theta|}\\(\theta_0\le\theta\le\pi-\theta_0)\end{cases}\tag{69}$$

$$f_{s\_\rm VOT}(\theta)=\begin{cases}\frac{V_m^2V_o}{4P_oL(V_o+V_m|\sin\theta|)^2}\\(0\le\theta<\theta_0\,\&\,\pi-\theta_0<\theta\le\pi)\\\frac{V_o^2(V_m|\sin\theta|-V_o)}{4P_oLV_m|\sin^3\theta|}\\(\theta_0\le\theta\le\pi-\theta_0)\end{cases}\tag{70}$$

$\rm CF_{off}\,(R_{gate})$ can be calculated as

$$\rm CF_{off}(R_{gate})=\frac{E_{off}(R_{gate})}{E_{off}(R_{gate(test)})}.\tag{71}$$

In the prototype, the gate drive resistance ($R_{\rm gate}$) is $2.2\,\Omega$. The value of $R_{\rm gate(test)}$, $E_{\rm off}(R_{\rm gate})$ and $E_{\rm off}(R_{\rm gate(test)})$ can be obtained from the datasheet of MOSFET.

The curve of the relationship between $E_{\rm off}$ and the current can be fitted with the following function, which is plotted in red in Fig. 5

$$Y(x)=0.0001041666x^2+0.001458333x+0.0025.\tag{72}$$

According to (21) in the application note [25, p. 23], for flyback and buck modes, $CF_{\rm off}(V_{\rm ds}(\rm off_{flyback}))$ can be expressed respectively as

$$CF_{\rm off}(V_{\rm ds}(\rm off_{flyback}))=\frac{10^{-4}\cdot(V_m|\sin\theta|+nV_o)+2.8\cdot10^{-3}}{0.043}\tag{73}$$

$$CF_{\rm off}(V_{\rm ds}(off_{\rm buck}))=\frac{10^{-4}\cdot(V_m|\sin\theta|)+2.8\cdot10^{-3}}{0.043}.\tag{74}$$

The substitution of (3), (12), (21), (31), and (69)–(74) into (67) and (68) leads to the turn-off loss.

4) *Copper loss of primary and secondary inductors:* For both primary and secondary windings of the inductor, the copper loss of the converter with COT and VOT controls can be calculated respectively as

$$P_{\rm copper(COT)}=I^2_{p\_\rm rms\_COT}R_{p\_\rm copper}+I^2_{s\_\rm rms\_COT}R_{s\_\rm copper}\tag{75}$$

$$P_{\rm copper(VOT)}=I^2_{p\_\rm rms\_VOT}R_{p\_\rm copper}+I^2_{s\_\rm rms\_VOT}R_{s\_\rm copper}\tag{76}$$

where $R_{p\_\rm copper}$ and $R_{s\_\rm copper}$ is the equivalent resistance of the primary and secondary windings respectively. Based on (3), (8), (12), (16), (21), (31), (55)–(62), (75) and (76), the copper loss can be obtained.

5) *Core loss of primary and secondary inductor:* According to Steinmetz equation [24], [26], the total core loss of primary and secondary inductors of the converter with COT and VOT controls can be calculated as

$$P_{t\_\rm core(COT)}=\frac{10^3\,V_e}{\pi}\left[\int_0^{\pi}\left(\begin{array}{l}C_m\,f_{s\_\rm COT}(\theta)^x B_{\rm ac\_COT}(\theta)^y\\\left(ct_0-ct_1T_a-ct_2T_a^2\right)d\theta\end{array}\right)\right]\tag{77}$$

$$B_{\rm ac\_COT}(\theta)=\begin{cases}\dfrac{L_p i_{\rm Lp\_pk\_COT}(\theta)}{2N_pA_e}\\(0\le\theta<\theta_0)\,\&\,(\pi-\theta_0<\theta\le\pi)\\\dfrac{L_s i_{\rm Ls\_pk\_COT}(\theta)}{2N_sA_e}(\theta_0\le\theta\le\pi-\theta_0)\end{cases}\tag{78}$$

$$P_{t\_\rm core(VOT)}=\frac{10^3\,V_e}{\pi}\left[\int_0^{\pi}\left(\begin{array}{l}C_m\,f_{s\_\rm VOT}(\theta)^x B_{\rm ac\_VOT}(\theta)^y\\\left(ct_0-ct_1T_a-ct_2T_a^2\right)d\theta\end{array}\right)\right]\tag{79}$$

$$B_{\rm ac\_VOT}(\theta)=\begin{cases}\dfrac{L_p i_{\rm Lp\_pk\_VOT}(\theta)}{2N_pA_e}\\(0\le\theta<\theta_0)\,\&\,(\pi-\theta_0<\theta\le\pi)\\\dfrac{L_s i_{\rm Ls\_pk\_VOT}(\theta)}{2N_sA_e}\,(\theta_0\le\theta\le\pi-\theta_0)\end{cases}\tag{80}$$

where $B_{\rm ac}(\theta)$ is the function of ac flux density through the magnetic core over the line period. N_p is the turns number of the primary inductor. V_e and A_e are the effective volume and area of the core, respectively. T_a is the environment temperature. C_m, x, y, ct_0, ct_1, and ct_2 are parameters found by curve fitting power loss measurement data. In the prototype, the Ferroxcube RM14 of 3F3 is selected as the magnetic core, whose parameters can be found from [27]–[29]. From (3), (12), (21), (31), (69), (70), and (77)–(80), the core loss can be calculated.

6) *Conduction loss of output diode:* The conduction loss of output diode for the converter with COT and VOT controls can

be determined as

$$P_{\text{con\_outputdiode(COT)}} = \frac{V_{\text{FD}_O}}{\pi} \int_0^{\pi} \frac{i_{\text{pk\_COT}}(\theta)}{2} (1 - D(\theta))\, d\theta \tag{81}$$

$$P_{\text{con\_outputdiode(VOT)}} = \frac{V_{\text{FD}_O}}{\pi} \int_0^{\pi} \frac{i_{\text{pk\_VOT}}(\theta)}{2} (1 - D(\theta))\, d\theta \tag{82}$$

where $D(\theta)$ is the duty cycle which is the ratio of on-time to the total time, its value from (8) and (16) is given below

$$D(\theta) = \times \begin{cases} \dfrac{1}{\left(1 + \dfrac{\sqrt{L_s} V_m |\sin\theta|}{\sqrt{L_p} V_o}\right)} (0 \le \theta < \theta_0)\ \&\ (\pi - \theta_0 < \theta \le \pi) \\ \dfrac{V_o}{V_m |\sin\theta|} \qquad (\theta_0 \le \theta \le \pi - \theta_0) \end{cases} \tag{83}$$

The value of V_{FDO} can be found from the datasheet of MUR1560. According to (3), (12), (21), (31), (69), (70), and (81)–(83), the conduction loss can be determined.

7) *Theoretical efficiency:* The theoretical efficiency of the converter with COT and VOT controls can be obtained as

$$\eta_{\text{COT}} = \frac{P_o}{\begin{pmatrix} P_o + P_{\text{con\_bridge(COT)}} + P_{\text{con\_switches(COT)}} \\ + P_{\text{off\_switches(COT)}} + P_{t\text{\_copper(COT)}} \\ + P_{t\text{\_core(COT)}} + P_{\text{con\_outputdiode(COT)}} \end{pmatrix}} \tag{84}$$

$$\eta_{\text{VOT}} = \frac{P_o}{\begin{pmatrix} P_o + P_{\text{con\_bridge(VOT)}} + P_{\text{con\_switches(VOT)}} \\ + P_{\text{off\_switches(VOT)}} + P_{t\text{\_copper(VOT)}} \\ + P_{t\text{\_core(VOT)}} + P_{\text{con\_outputdiode(VOT)}} \end{pmatrix}}. \tag{85}$$

From the specifications of the converter given in Section V, the theoretical efficiency is obtained and shown in Fig. 6. It can be seen that, for turns ratio 1 and 2, the efficiency of the converter with VOT control is increased at low input voltage and slightly decreased at high input voltage, compared to that with COT control.

V. Experimental Verification

In order to verify the validity of the proposed VOT control scheme, a prototype for turns ratio one has been built and tested in the lab. The intended application is low power conversion such as high brightness LED power supply and metal halide lamp where high PF for the universal input is required [24], [30]. The specifications and the main components of the prototype are as follows.

Input voltage v_{in}: 90–264 VAC; line frequency f_{line}: 50 Hz; output voltage V_o: 80 V; output power P_o: 100 W; output current 1.25 A; input bridge rectifier: KBL10; power switches Q_1 and

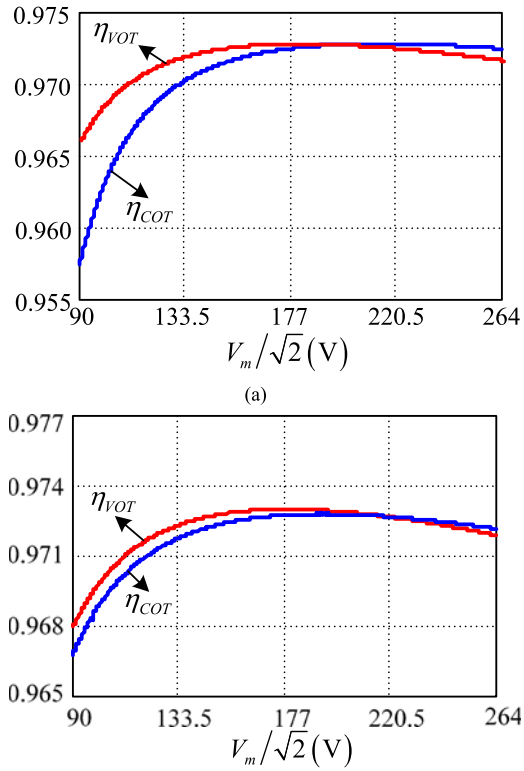

Fig. 6. Calculated efficiency for whole input voltage range and full load: (a) $n = 1$ and (b) $n = 2$.

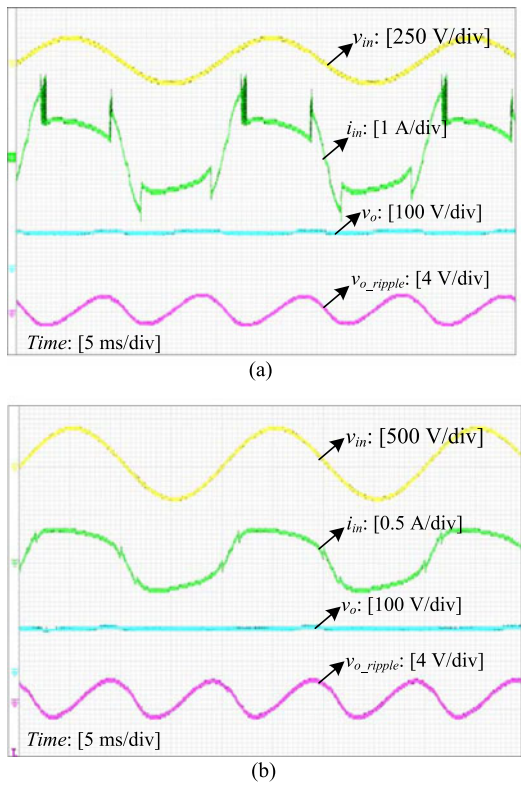

Fig. 7. Experimental waveforms with COT control: (a) 90 VAC and (b) 264.

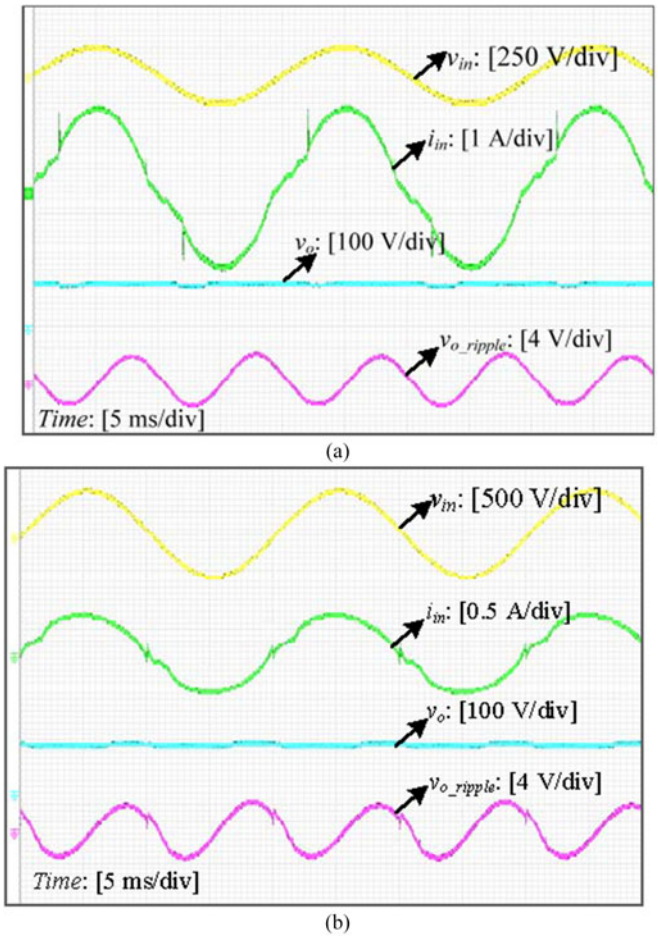

Fig. 8. Experimental waveforms with VOT control: (a) 90 VAC and (b) 264.

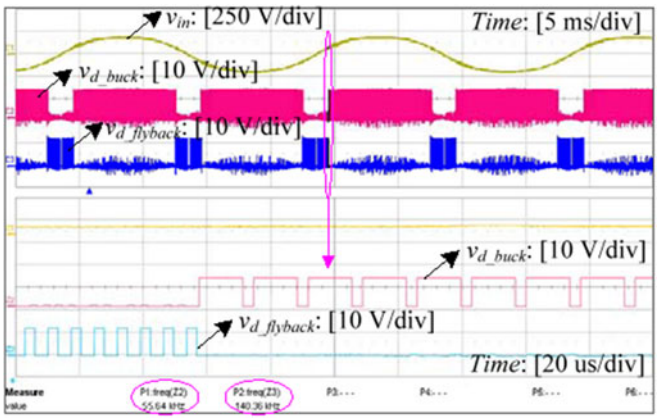

Fig. 9. Switch gate drive signals of the converter with VOT at 120 VAC at the transition from the flyback to buck mode.

Q_2: 20N60C3; output diode D_o: MUR1560; primary inductance $L_{\rm p}$: 118 μH; secondary inductance L_s: 118 μH; output capacitor C: 1000 μF; control IC: L6561.

Figs. 7 and 8 illustrate the experimental waveforms of the input voltage, input current, output voltage, and output voltage ripple of the converter with COT and VOT controls at 90, and 264 VAC inputs, respectively. It can be seen that compared to that with COT control, the input current with VOT control is more sinusoidal at all input voltages. Also, the peak-to-peak values of the output voltage ripple agree well with theoretical results in Section IV-A.

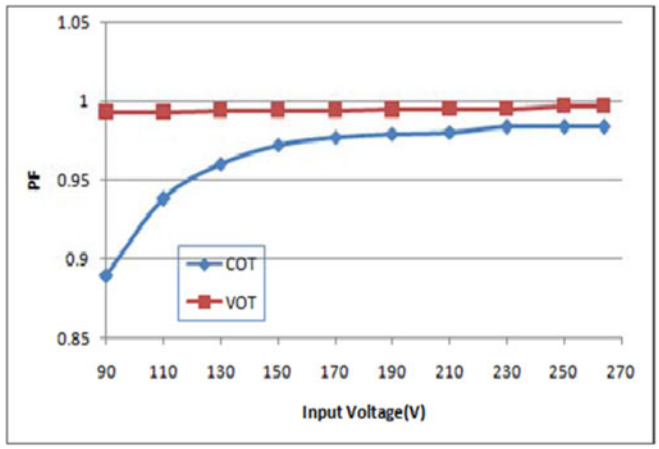

Fig. 10. Measured PF.

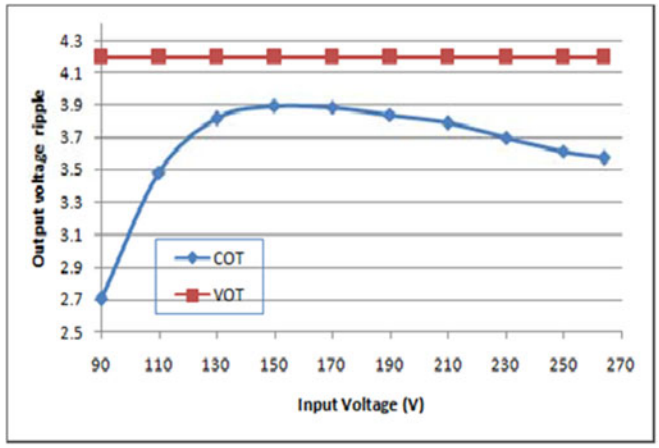

Fig. 11. Measured output ripple.

Fig. 9 shows the switches' gate drive signals of the converter at the transition from flyback to buck, from which it can be seen that the converter operates either in the buck mode or in the flyback mode depending on the boundary voltage and the transition, between the buck and flyback modes is smooth.

Fig. 10 shows the measured input PF, which demonstrate that as VOT control is employed for the converter, the input PF is increased to nearly unity within the wide input voltage range.

Fig. 11 illustrates the measured output voltage ripple of COT and VOT controls, from which it can be seen that output voltage ripple in VOT control is slightly more.

Fig. 12 illustrates the measured efficiency of the converter, from which it can be seen that VOT control achieves higher efficiency especially at low line input voltage. The measured results nearly agree with that of the theoretical analysis shown in Fig. 6.

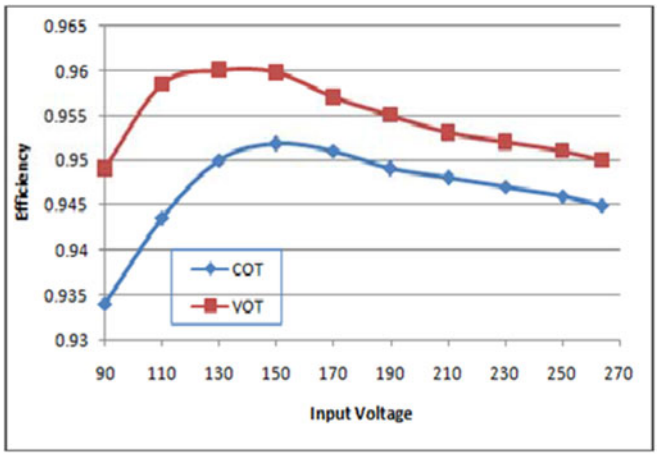

Fig. 12. Measured efficiency.

VI. Conclusion

A VOT control scheme is proposed in this paper so as to make the shape of average input current purely sinusoidal for the CRM buck–flyback PFC converter. The analysis and experimental results are given. Compared with that of the COT control:

1) PF is nearly unity and THD is low within the wide input voltage range;
2) efficiency is increased especially at low input voltage.

References

[1] O. Garcia, J. A. Cobos, R. Prieto, P. Alou, and J. Uceda, "Single phase power factor correction: A survey," *IEEE Trans. Power Electron.*, vol. 18, no. 3, pp. 749–755, May 2003.

[2] F. Musavi, M. Edington, W. Eberle, and W. G. Dunford, "Evaluation and efficiency comparison of front end AC-DC plug-in hybrid charger topologies," *IEEE Trans. Smart Grid*, vol. 3, no. 1, pp. 413–421, Mar. 2012.

[3] K. Yao, W. Hu, Q. Li, and J. Lyu, "A novel control scheme of DCM boost PFC converter," *IEEE Trans. Power Electron.*, vol. 30, no. 10, pp. 5605–5615, Oct. 2015.

[4] Y. Tang, D. Zhu, C. Jin, P. Wang, and F. Blaabjerg, "A three-level quasi-two-stage single-phase pfc converter with flexible output voltage and improved conversion efficiency," *IEEE Trans. Power Electron.*, vol. 30, no. 2, pp. 717–726, Feb. 2015.

[5] H.-S. Kim, J.-K. Kim, K.-B. Park, and H.-W. Seong, "On/off control of boost PFC converters to improve light-load efficiency in paralleled power supply units for servers," *IEEE Trans. Ind. Electron.*, vol. 61, no. 3, pp. 1235–1242, Mar. 2014.

[6] C. Marxgut, F. Krismer, D. Bortis, J. W. Kolar, "ultraflat interleaved triangular current mode (TCM) single-phase PFC rectifier," *IEEE Trans. Power Electron.*, vol. 29, no. 2, pp. 873–882, Feb. 2014.

[7] Y. Yang, X. Ruan, J. He, and Z. Ye, "Feed-forward scheme for an electrolytic capacitor-less AC/DC LED driver to reduce output current ripple," *IEEE Trans. Power Electron.*, vol. 29, no. 10, pp. 5508–5518, Oct. 2014.

[8] T. Yan, J. Xu, F. Zhang, J. Sha, and Z. Dong, "Variable-on-time-controlled critical-conduction-mode flyback PFC converter," *IEEE Trans. Ind. Electron.*, vol. 61, no. 11, pp. 6091–6099, Nov. 2014.

[9] Y. Cho and J.-S. Lai, "Digital plug-In repetitive controller for single-phase bridgeless PFC converters," *IEEE Trans. Power Electron.*, vol. 28, no. 1, pp. 165–175, Jan. 2013.

[10] K. I. Hwu and Y. T. Yau, "An interleaved ac–dc converter based on current tracking," *IEEE Trans. Ind. Electron.*, vol. 56, no. 5, pp. 1456–1463, May 2009.

[11] K. Yao, X. Ruan, X. Mao, and Z. Ye, "Variable-duty-cycle control to achieve high input power factor for DCM boost PFC converter," *IEEE Trans. Ind. Electron.*, vol. 58, no. 5, pp. 1856–1865, May 2011.

[12] F. Sichirollo, J. Marcos Alonso, and G. Spiazzi, "A novel double integrated buck offline power supply for solid-state lighting applications," *IEEE Trans. Ind. Appl.*, vol. 51, no. 2, pp. 1268–1276, Mar./Apr. 2015.

[13] Y. Ohnuma and J.-I. Itoh, "A novel single-phase buck PFC AC–DC converter with power decoupling capability using an active buffer," *IEEE Trans. Ind. Appl.*, vol. 50, no. 3, pp. 1905–1914, May./Jun. 2014.

[14] A. A. Fardoun, E. H. Ismail, N. M. Khraim, A. J. Sabzali, and M. A. Al-Saffar, "Bridgeless high-power-factor buck-converter operating in discontinuous capacitor voltage mode," *IEEE Trans. Ind. Appl.*, vol. 50, no. 5, pp. 3457–3467, Sep./Oct. 2014.

[15] T. B. Soeiro, T. Friedli, and J. W. Kolar, "design and implementation of a three-phase buck-type third harmonic current injection PFC rectifier SR," *IEEE Trans. Power Electron.*, vol. 28, no. 4, pp. 1608–1621, Apr. 2013.

[16] L. Huber, L. Gang, and M. M. Jovanović, "Design-oriented analysis and performance evaluation of buck PFC front end," *IEEE Trans. Power Electron.*, vol. 25, no. 1, pp. 85–94, Jan. 2010.

[17] Y. Jang and M. M. Jovanović, "Bridgeless high-power-factor buck converter," *IEEE Trans. Power Electron*, vol. 26, no. 2, pp. 602–611, Feb. 2011.

[18] Y. Chen, Y. Nan, and Q. Kong, "A loss-adaptive self-oscillating buck converter for LED driving," *IEEE Trans. Power Electron.*, vol. 7, no. 10, pp. 4321–4328, Oct. 2012.

[19] C.-Y. Chiang and C.-L. Chen, "Zero-voltage-switching control for a PWM buck converter under DCM/CCM boundary," *IEEE Trans. Power Electron.*, vol. 24, no. 9, pp. 2120–2126, Sep. 2009.

[20] J.-H. Park and B.-H. Cho, "The zero voltage switching (ZVS) critical conduction mode (CRM) buck converter with tapped-inductor," *IEEE Trans. Power Electron.*, vol. 20, no. 4, pp. 762–774, Jul. 2005.

[21] J. Yang, X. Wu, J. Zhang, and Z. Qian, "Design considerations of a high efficiency ZVS buck AC-DC converter with constant on-time control," in *Proc. IEEE 32nd Int. Telecommun. Energy Conf.*, 2010, pp. 1–5.

[22] X. Wu, J. Yang, J. Zhang, and M. Xu, "Design considerations of a high efficiency soft-switched buck AC-DC converter with constant on-time (COT) control," *IEEE Trans. Power Electron.*, vol. 26, no. 11, pp. 3144–3152, Nov. 2011.

[23] X. Wu, J. Yang, J. Zhang, and Z. Qian, "Variable on-time (VOT) controlled critical conduction, mode buck PFC converter for high input Ac/Dc HBLED lighting application," *IEEE Trans. Power Electron.*, vol. 27, no. 11, pp. 3144–3152, Nov. 2012.

[24] X. Xie, C. Zhao, Q. Lu, and S. Liu, "Novel integrated buck–flyback nonisolated PFC converter with high power factor," *IEEE Trans. Ind. Electron.*, vol. 60, no. 12, pp. 5603–5612, Dec. 2013.

[25] Infineon Application Note, "How to select the right CoolMOS and its power handling capability," V1.2, Jan. 2002.

[26] J. Mühlethaler, J. Bielay, J. W. Kolar, and A. Ecklebez, "Improved core-loss calculation for magnetic components employed in power electronics systems," *IEEE Trans. Power Electron.*, vol. 27, no. 2, pp. 964–973, Feb. 2012.

[27] Ferroxocube Application Note, "Design of planar power transformer," May 1997.

[28] Ferroxocube Data Sheet, "RM14/ILP, RM, RM/I, RM/ILP cores and accessories," Sep. 2004.

[29] W. Inam, K. K. Afridi, and D. J. Perreault, "High efficiency resonant dc/dc converter utilizing a resistance compression network," *IEEE Trans. Power Electron.*, vol. 29, no. 8, pp. 4126–4136, Aug. 2014.

[30] M. A Dalla Costa, J. M Alonso, J. M Alonso, J. C. Miranda, J. Garcia, and D. G Lamar, "A single-stage high power-factor electronic ballast based on integrated buck–flyback converter to supply metal halide lamps," *IEEE Trans. Ind. Electron.*, vol. 55, no. 3, pp. 1112–1122 Mar. 2008.

Abdul Hakeem Memon was born in Sindh, Pakistan, in 1987. He received the B.E. and M.E. degrees in electrical engineering from Mehran University of Engineering and Technology, Jamshoro, Sindh, Pakistan, in 2009 and 2013, respectively, where he is working as a Lecturer. He is currently working toward the Ph.D. degree in power and automation engineering from Nanjing University of Science and Technology, Nanjing, China.

His research interests include power factor correction converters, soft-switching techniques, and high efficiency ac–dc and dc–dc converter.

Kai Yao (M'14) was born in Jiangsu, China, in 1980. He received the B.S. degree in industrial automation from Nantong University, Nantong, China, in 2002, the M.S. degree in mechanical design and theory, and the Ph.D. degree in electrical engineering from Nanjing University of Aeronautics and Astronautics, Nanjing, China, in 2005 and 2010, respectively. In 2011, he joined the Faculty of Electrical Engineering, School of Automation, Nanjing University of Science and Technology, where he has been engaged in teaching and research in the field of power electronics.

His research interests include power factor correction converters, renewable energy generation system, and power supplies for LED.

Qingwei Chen was born in Jiangsu, China, in 1963. He received the B.S. degree in industrial electrical automation from the Department of Electrical Engineering, Jiangsu University, Zhenjiang, China, in 1985. He received the M.S. degree in automatic control theory and application and Ph.D. degree in control science and engineering from Nanjing University of Science and Technology, Nanjing, China, in 1988 and 2005 respectively.

From 1988 to 2001, he was a Teaching Assistant, a Lecturer, and an Associate Professor in the School of Automation, Nanjing University of Science and Technology, where he is currently a Professor. His research interests include motor power driver, control of servo system, and multi-objective optimization.

Jian Guo received the B.S. degree in electrical technology and Ph.D. degree in control theory and control engineering from Nanjing University of Science and Technology, Nanjing, China, in 1997 and 2002, respectively. Since 2002, he has been with the School of Automation, Nanjing University of Science and Technology, and was promoted as a Professor in 2013.

His research interests include power electronic, intelligent system, and motion control.

Wenbin Hu was born in Jiangsu, China, in 1970. He received the B.S. degree in electrical engineering and automation from the Nanjing University of Aeronautics and Astronautics, Nanjing, China, in 1992, the M.S. degree in control theory and control engineering from the Nanjing University of Science and Technology (NUST), Nanjing, China, in 1999, and the Ph.D. degree in electrical engineering from the Nanjing University of Aeronautics and Astronautics, in 2003. In 2004, he joined the Faculty of Electrical Engineering, School of Automation, NUST. In 2010, he became an Associate Professor at NUST, where he has been engaged in teaching and research in the field of power electronics.

His research interests include power factor correction converters, renewable energy generation systems, and electric traction systems for rail vehicles.